Dual-probe near-field fiber head with gap servo control for data storage applications

Jen-Yu Fang[1], Chung-Hao Tien[2], and Han-Ping D. Shieh[2]

[1]*Department of Photonics and Institute of Electro-Optical Engineering*
[2]*Department of Photonics and Display Institute, National Chiao Tung University, Hsinchu 30010, Taiwan*
ryfang.eo91g@nctu.edu.tw

Abstract: We present a novel fiber-based near-field optical head consisting of a straw-shaped writing probe and a flat gap sensing probe. The straw-shaped probe with a C-aperture on the end face exhibits enhanced transmission by a factor of 3 orders of magnitude over a conventional fiber probe due to a hybrid effect that excites both propagation modes and surface plasmon waves. In the gap sensing probe, the spacing between the probe and the disk surface functions as an external cavity. The high sensitivity of the output power to the change in the gap width is used as a feedback control signal. We characterize and design the straw-shaped writing probe and the flat gap sensing probe. The dual-probe system is installed on a conventional biaxial actuator to demonstrate the capability of flying over a disk surface with nanometer position precision.

OCIS codes: (220.4830) Optical systems design; (050.1220) Apertures; (060.2280) Fiber design and fabrication; (280.3420) Laser sensors; (210.0210) Optical data storage

References and links

1. D. W. Pohl, W. Denk, and M. Lanz, "Optical stethoscopy: image recording with resolution λ/20," Appl. Phys. Lett. **44**, 651-653 (1984).
2. E. Betzig and J. K. Trautman, "Near-field optics: microscopy, spectroscopy, and surface modification beyond the diffraction limit," Science **257**, 189-195 (1992).
3. B. D. Terris, H. J. Mamin, and D. Rugar, "Near-field optical data storage," Appl. Phys. Lett. **68**, 141-143 (1995).
4. X. Luo and T. Ishihara, "Subwavelength photolithography based on surface-plasmon polariton resonance," Opt. Express **14**, 3055-3065 (2004).
5. B. D. Terris, H. J. Mamin, D. Rugar, W. R. Studenmund, and G. S. Kino, "Near-field optical data storage using a solid immersion lens," Appl. Phys. Lett. **65**, 388-390 (1994).
6. W.-H. Yeh and M. Mansuripur, "Evanescent coupling in magneto-optical and phase-change disk systems based on the solid immersion lens," Appl. Opt. **39**, 302-315 (2000).
7. F. Guo, T. E. Schlesinger, and D. D. Stancil, "Optical field study of near-field optical recording with a solid immersion lens," Appl. Opt. **39**, 324-332 (2000).
8. T. Ishimoto, K. Saito, M. Shinoda, T. Kondo, A. Nakaoki, and M. Yamamoto, "Gap servo system for a biaxial device using an optical gap signal in a near field readout system," Jpn. J. Appl. Phys. **42**, 2719-2724, (2003).
9. J. I. Lee, M. A. H. van der Aa, C. A. Verschuren, F. Zijp, and M. B. van der Mark, "Development of an air gap servo system for high data transfer rate near field optical recording," Jpn. J. Appl. Phys. **44**, 3423-3426 (2005).
10. T. Yatsui, M. Kourogi, and M. Ohtsu, "Increasing throughput of a near-field optical fiber probe over 1000 times by the use of a triple-tapered structure," Appl. Phys. Lett. **73**, 2090–2092 (1998).
11. P. N. Minh, T. Ono, H. Watanabe, S. S. Lee, Y. Haga, and M. Esashi, "Hybrid optical fiber-apertured cantilever near-field probe," Appl. Phys. Lett. **79**, 3020–3022 (2001).
12. G. M. Kim, B. J. Kim, E. S. Ten Have, F. Segerink, N. F. Van Hulst, and J. Brugger, "Photoplastic near-field optical probe with sub-100 nm aperture made by replication from a nanomould," J. Microsc. **209**, 267–271 (2002).
13. P. A. Dechant, S. K. Dew, S. E. Irvine, and A. Y. Elezzabi, "High-transmission solid-immersion apertured optical probes for near-field scanning optical microscopy," Appl. Phys. Lett. **86**, 013102(3) (2005).
14. C.-H. Tien, Y.-C. Lai, T. D. Milster, and H.-P. D. Shieh, "Design and fabrication of fiberlenses for optical recording applications," Jpn. J. Appl. Phys. **41**, 1834-1837 (2002).
15. C.-H. Tien, H.-L. Chou, Y. Chiu, W. Hsu, T. D. Milster, Y.-C. Lai, and H.-P. D. Shieh, "Fiber-lens-based module for optical recording applications," Jpn. J. Appl. Phys. **42**, 4345-4348 (2003).

#84512 - $15.00 USD Received 25 Jun 2007; revised 31 Aug 2007; accepted 6 Sep 2007; published 22 Oct 2007

16. Y.-J Kim, K. Suzuki, and K. Goto, "Parallel recording array head of nano-aperture flat-tip probes for high-density near-field optical data storage," Jpn. J. Appl. Phys. **40**, 1783-1789 (2001).
17. M. Hirata, M. Oumi, K. Nakajima, and T. Ohkubo, "Near-field optical flying head with protruding aperture and its fabrication," Jpn. J. Appl. Phys. **44**, 3519-3523 (2005).
18. A. V. Itagi, D. D. Stancil, J. A. Bain, and T. E. Schlesinger, "Ridge waveguide as a near-field optical source," Appl. Phys. Lett. **83**, 4474-4476 (2003).
19. X. Shi, R. L. Thornton, and L. Hesselink, "Ultrahigh light transmission through a C-shaped nanoaperture," Opt. Lett. **28**, 1320-1322 (2003).
20. X. Shi and L. Hesselink, "Design of a C aperture to achieve λ/10 resolution and resonant transmission," J. Opt. Soc. Am. B **21**, 1305-1317 (2004).
21. L. Sun and L. Hesselink, "Low-loss subwavelength metal C-aperture waveguide," Opt. Lett. **31**, 3606-3608 (2006).
22. K. Sendur, W. Challener, and C. Peng, "Ridge waveguide as a near field aperture for high density data storage," J. Appl. Phys. **96**, 2743-2752 (2004).
23. Y.-C. Chen, J.-Y. Fang, C.-H. Tien, and H.-P. D. Shieh," High-transmission hybrid-effect-assisted nanoaperture," Opt. Lett. **31**, 655-657 (2006).
24. Y.-C. Chen, J.-Y. Fang, C.-H. Tien, and H.-P. D. Shieh, "Double-corrugated c-shaped aperture for near-field recording," Jpn. J. Appl. Phys. **45**, 1348-1350 (2006).
25. Y. Xie, A. R. Zakharian, J. V. Moloney and M. Mansuripur, "Optical transmission at oblique incidence through a periodic array of sub-wavelength slits in a metallic host," Opt. Express **14**, 10220-10227 (2006).
26. P.-K Wei, Y.-C. Huang, C.-C. Chieng, F.-G. Tseng and W. Fann, "Off-angle illumination induced surface plasmon coupling in subwavelength metallic slits," Opt. Express **13**, 10784-10794 (2005).
27. H. Raether: *Surface Plasmons on Smooth and Rough Surfaces and on Gratings* (Springer, New York, 1988)
28. G. Giuliani, M. Norgia, S. Donati, and T. Bosch, "Laser diode self-mixing technique for sensing applications," J. Opt. A: Pure Appl. Opt. **4**, S283–S294 (2002).
29. R. O. Miles, A. Dandridge, A. B. Tveten, and T. G. Gialloenzi, "An external cavity diode laser sensor," J. Lightwave Technol. **LT-1**, 81-93 (1983).
30. J.-Y. Kim and H. C. Hsieh, "An open-resonator model for the analysis of a short external-cavity laser diode and its application to the optical disk head," J. Lightwave Technol. **10**, 439-447 (1992).
31. J.-Y. Kim and H. C. Hsieh, "Asymmetry in the optical output power characteristics of a short-external-cavity laser diode," IEEE Photon. Technol. Lett. **4**, 537-539 (1992).

1. Introduction

Achieving spatial resolution beyond the diffraction limit is of critical importance in many fields, such as data storage, optical measurement, and lithography. Near-field optics opens an avenue to break through the diffraction limit [1-4]. However, low power transmission accompanies a decrease in spot size and nano-scale gap servo control is also necessary to maintain objective lenses or light sources in close proximity to target surfaces. Solid immersion lens (SIL) was demonstrated to be able to reduce spot size by a factor of the refractive index of the SIL material in data storage [5-7]. An external optical system had to be implemented to deliver and deal with optical signals [8, 9]. The configuration was also bulky and difficult to integrate with other systems. Another approach was to employ a fiber probe in collecting light from the target [10-15]. The spacing between the probe and the target surface was kept constant by monitoring the change in the oscillation of the probe resulted from shear force on the probe as a function of the spacing. Because the transmission of conventional fiber probes with a 100-nm aperture was around 10^{-5}, a signal processing system was necessary to filter out background noise. In addition, to miniaturize the optical system to improve dynamic response and integration capability, integrated waveguides were also presented [16-18]. However, fabrication processes were complex and not easily mass produced economically.

To achieve high resolution and efficiency, miniaturization, and active gap servo control, we propose a dual-probe near-field fiber head system consisting of a straw-shaped writing probe that delivers optical power to the disk and a gap sensing probe that detects the spacing and sends a feedback signal to the controller. The configuration of the system with two independent optical paths is schematically illustrated in Fig. 1. In the writing probe, a 1×2 10/90 fiber coupler is inserted into the optical path to split the light into two. 90% of the light goes to the straw-shaped probe, where the end face is coated with a metallic film and perforated by a C-aperture at the center; while the remaining light goes to the bare flat reference probe where we measure the emitted power to derive the output from the straw-shaped probe. In the gap sensing probe, the spacing between the probe end and the target surface functions as an external cavity for the laser diode. The interference between the

#84512 - $15.00 USD Received 25 Jun 2007; revised 31 Aug 2007; accepted 6 Sep 2007; published 22 Oct 2007

reflected light and the field inside the laser cavity makes the output power dependent on the gap width. The output power modulated by the gap width is detected by the photodiode and sent to the controller as a feedback signal. The dual-probe fiber head is installed on a conventional biaxial actuator driven by the controller to maintain the gap with nanometer position precision.

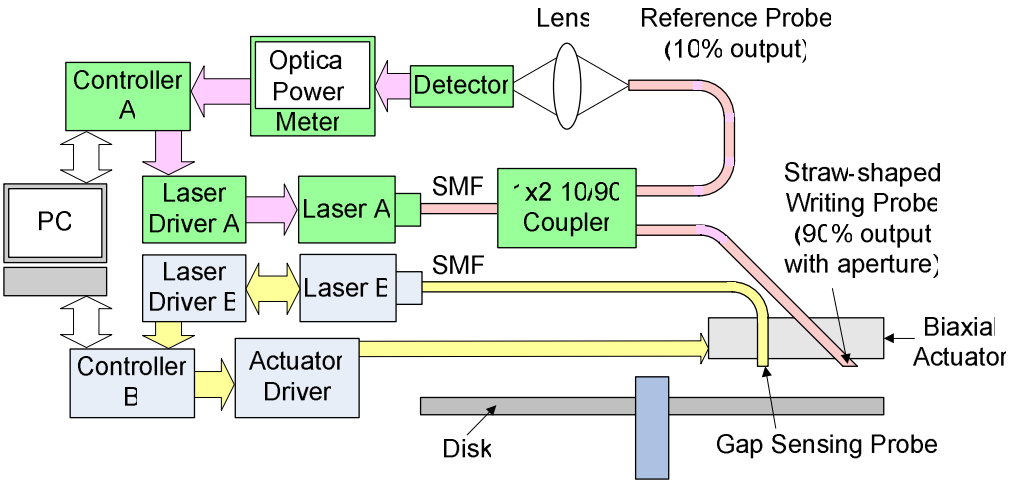

Fig. 1. Configuration of a dual-probe near-field fiber-based light delivery system

In this paper, we calculate the transmission of a C-shaped nano-aperture with oblique incidence to characterize and design the straw-shaped fiber probe. In addition, a self-mixing interferometric signal as a function of the gap width is modeled and measured for controller design. Consequently, a straw-shaped fiber probe with a 45-degree angle and a gap sensing probe are fabricated and installed on a conventional biaxial actuator. The experimental results demonstrate the performance of the system on a moving disk surface.

2. System characterization and design

2.1 Straw-shaped writing probe

A C-shaped nano-aperture which functions as a ridge waveguide supports propagation modes and thus sufficiently increases the transmission through the aperture [18-22]. To further enhance the transmission through a C-aperture in a near-field light source system, we demonstrated a nano-aperture surrounded by a periodic corrugation can induce a hybrid effect consisting of propagation modes and surface plasmon excitation [23, 24]. Because the surface plasmon is able to be excited with oblique incidence [25, 26], we propose that a C-aperture with oblique incident illumination can also induce the hybrid effect. The optical model is schematically plotted in Fig. 2(a). A transverse-magnetic (TM) plane wave illuminates the aperture in a 200-nm silver film with a complex refractive index of N=0.135+3.988i from a dielectric substrate with N=1.475 at a free-space incident wavelength λ=633 nm. The dimensions of the C-aperture are shown in Fig. 2(b). The power throughput (PT) is defined as the ratio of the transmitted optical power out of an aperture to the incident power over the aperture area to represent the photon capturing capability. An aperture with the PT greater than 1 implies some photons obstructed behind the film can be captured by the aperture and go through the aperture. Therefore, to investigate the interaction between the aperture and the incident light, the PT of the C-shaped nano-aperture with oblique incidence is calculated as an optimized parameter by employing the Finite-Difference Time Domain method (FDTD).

#84512 - $15.00 USD Received 25 Jun 2007; revised 31 Aug 2007; accepted 6 Sep 2007; published 22 Oct 2007

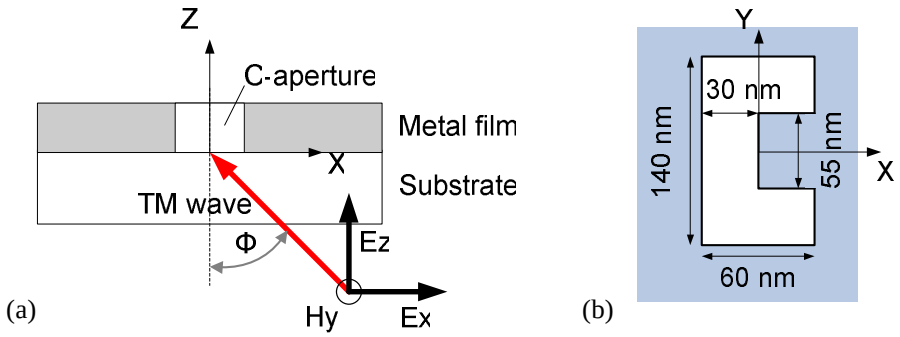

Fig. 2. (a). Schematic illustration of the optical model and (b) the dimensions of the C-aperture

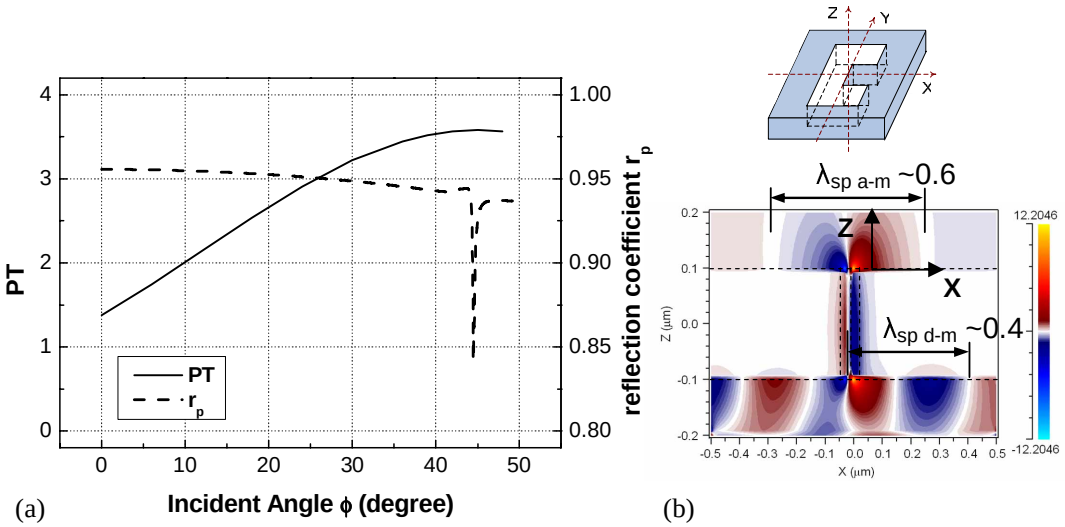

Fig. 3. (a). The power throughput (PT) at a distance of 50 nm from the aperture and reflection coefficient r_p as a function of the incident angle and (b) Calculated E_z field profile in XZ plane when the incident angle was 44 degree. The dashed line shows the contour of the metal film and the C-aperture.

The power throughput as a function of the incident angle is shown in Fig. 3(a). The calculated power throughput exhibits a peak of 3.5 at a 44-degree incidence which coincides with the position of a dip in the refection coefficient where attenuated total reflection (ATR) occurs. In contrast to the power throughput of 1.4 with normal incidence, the maximum power throughput yields an enhancement as high as 2.5. According to surface plasmon theory, the coincidence indicates that the excitation of surface plasmon in the dielectric-metal interface contributes to the power throughput enhancement with oblique incidence. The calculated *Ez* field profile in *XZ* plane at 44-degree incidence, as shown in Fig. 3(b), further reveals the surface plasmon excitation in the dielectric-metal interface induced by the incident electric field component perpendicular to the surface. The wavelength of the surface plasmon wave along *x* direction can be obtained by [27]

$$\lambda_{SP} = \frac{2\pi}{k_x} \tag{1}$$

The wave vector component along *x* direction k_x is

#84512 - $15.00 USD Received 25 Jun 2007; revised 31 Aug 2007; accepted 6 Sep 2007; published 22 Oct 2007

$$k_x = k_0 \left(\frac{\varepsilon_m \cdot \varepsilon_d}{\varepsilon_m + \varepsilon_d}\right)^{1/2} \tag{2}$$

where ε_m is the dielectric constant of the metal film, ε_d is that of the dielectric material, and k_0 is the wave vector of incident light. The calculated wavelength at the dielectric-metal interface $\lambda_{sp\,d\text{-}m}$ is 0.39 μm and at the air-metal interface $\lambda_{sp\,a\text{-}m}$ is 0.61 μm, which agree with the FDTD simulation results. Therefore, according to our simulation, a 45-degree straw-shaped fiber probe is proposed. The oblique incident illumination on a C-shaped aperture induces the excitation of the surface plasmon wave in the dielectric-metal interface and further enhances the transmission through the aperture. Compared to the calculated power throughput of a square aperture of 10^{-3} employing FDTD, the straw-shaped fiber probe provides an enhancement by a factor of $3x10^3$.

2.2 Gap Sensing Probe

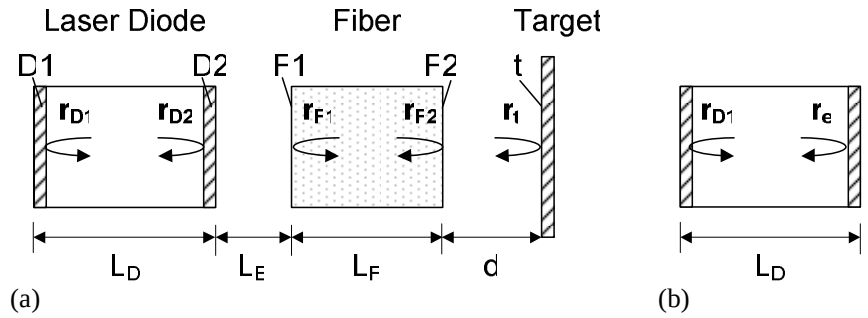

Fig. 4. (a). Configuration of an external-cavity laser diode with a length of fiber and (b) an equivalent laser diode

By means of the self-mixing interferometric effect, laser diodes can function as position sensors [28]. However, to further improve integration capability and dynamic response characteristics, a length of fiber is attached to the laser diode sensor as a gap sensing probe. To characterize the feedback signal from the gap sensing probe, we consider a laser diode of length L_D connected to a single-mode fiber (SMF) of length L_F and a target surface being gap d in front of the fiber end, as shown in Fig. 4(a). Because the displacement of the target surface and the spacing are assumed to be a few wavelengths, i.e. $\Delta d << L_D$ and $d << L_D$, the change in the cavity modes caused by the presence and movement of the target surface is ignored [29]. To characterize the modulation in output power as a function of the gap between the target surface and the fiber end, an equivalent laser diode with effective reflectivity r_e in terms of reflection coefficients and complex coupling coefficient C_n is employed [30, 31]. The coupling coefficient C_n represents the ratio of reflected light coupling into the laser diode at the nth reflection and is a complex function of the external cavity length representing both phase shift and amplitude reduction. The equavilent gap sensing system is shown in Fig. 4(b). The effective reflectivity is written as

$$r_e = r_{D2} - \frac{(1-R_{D2})}{r_{D2}} \sum_{n=1}^{\infty} [C_{n1}(-r_{D2} \cdot r_{F1} \cdot e^{i\phi_{F1}})^n + C_{n2}(-r_{D2} \cdot r_{F2} \cdot (1-R_{F1})^2 \cdot e^{i\phi_{F2}})^n + C_{n3}(-r_{D2} \cdot r_t \cdot (1-R_{F1})^2 \cdot (1-R_{F2})^2 \cdot e^{i\phi_t})^n], \tag{3}$$

where r_{D1}, r_{D2}, r_{F1}, r_{F2}, and r_t denote the amplitude reflection coefficients of the laser facets, fiber facets, and the external reflector, R_{D2}, R_{F1}, and R_{F2} denote the power reflectivity of the laser diode facet and fiber facets, and Φ_{F1}, Φ_{F2}, and Φ_t, denote the phase shift resulted from

#84512 - $15.00 USD Received 25 Jun 2007; revised 31 Aug 2007; accepted 6 Sep 2007; published 22 Oct 2007

the optical path difference between the laser cavity and the reflecting surfaces F1, F2, and t, respectively.

$$R_i = \left|r_i\right|^2, \quad \text{where } i = D1, D2, F1, \text{ and } F2. \tag{4}$$

The phase shift Φ resulted from the spacing

$$\phi = \frac{4\pi \cdot d}{\lambda}. \tag{5}$$

If we assume the reflectivity of the fiber facets is much less than 1, either $(1-R_{F1})$ or $(1-R_{F2})$ can be approximated by 1. The effective reflectivity can be obtained as follows

$$r_e = r_{D2} - \frac{(1-R_{D2})}{r_{D2}} \sum_{n=1}^{\infty} [C_{n1}(-r_{D2} \cdot r_{F1} \cdot e^{i\phi_{F1}})^n + C_{n2}(-r_{D2} \cdot r_{F2} \cdot e^{i\phi_{F2}})^n + C_{n3}(-r_{D2} \cdot r_t \cdot e^{i\phi_t})^n]. \tag{6}$$

Because the reflectivity coefficient term decreases more rapidly than the coupling coefficient as the reflection increases, the reflectivity coefficient term from the target surface dominates the amplitude. The coupling coefficient is regarded as a function of the spacing *d* and independent on the reflection. Then the effective reflectivity can be derived as below:

$$\begin{aligned} r_e &= r_{D2} - \frac{(1-R_{D2})C_{n1}}{r_{D2}} \sum_{n=1}^{\infty} (-r_{D2} \cdot r_{F1} \cdot e^{i\phi_{F1}})^n - \frac{(1-R_{D2})C_{n2}}{r_{D2}} \sum_{n=1}^{\infty} (-r_{D2} \cdot r_{F2} \cdot e^{i\phi_{F2}})^n \\ &\quad - \frac{(1-R_{D2})C_{n3}}{r_{D2}} \sum_{n=1}^{\infty} (-r_{D2} \cdot r_t \cdot e^{i\phi_t})^n \\ &= r_{D2} - \frac{(1-R_{D2})C_{n1} \cdot r_{F1} \cdot e^{i\phi_{F1}}}{1 + r_{D2} \cdot r_{F1} \cdot e^{i\phi_{F1}}} - \frac{(1-R_{D2})C_{n2} \cdot r_{F2} \cdot e^{i\phi_{F2}}}{1 + r_{D2} \cdot r_{F2} \cdot e^{i\phi_{F2}}} \\ &\quad - \frac{(1-R_{D2})C_{n3} \cdot r_t \cdot e^{i\phi_d}}{1 + r_{D2} \cdot r_t \cdot e^{i\phi_d}}. \end{aligned} \tag{7}$$

If we assume the reflectivity of the target surface is much higher than that of the fiber facets, i.e. $r_t >> r_{F1} = r_{F2}$, the second and third term of Eq. (7) can be ignored. Then a simplified formula can be obtained

$$r_e = r_{D2} - \frac{(1-R_{D2})C_{n3} \cdot r_t \cdot e^{i\phi_d}}{1 + r_{D2} \cdot r_t \cdot e^{i\phi_d}}. \tag{8}$$

If we assume a constant current applied to the laser diode, the output power can be represented in terms of the applied current *I* and the threshold current I_{th} which is a function of the effective reflectivity

$$P_e \propto (I - I_{th}) \propto [P_C - \ln(\frac{1}{\sqrt{R_{D1} \cdot R_e}})], \tag{9}$$

where P_C is a constant. In the case of r_{D1} = 0.99, r_{D2} = 0.9, r_t = 0.8, and λ = 0.635 μm, we calculate the power output as a function of the spacing between the laser and the target surface according to the equations derived above, as shown in Fig. 5. Because the absolute value of

#84512 - $15.00 USD Received 25 Jun 2007; revised 31 Aug 2007; accepted 6 Sep 2007; published 22 Oct 2007

output signals is highly dependent on gain of the control system, we normalize both measured and calculated signals to unity by being divided by the maximum value and convert them to a function of relative position in terms of wavelength. The comparison shows that the proposed model agrees well with the measurement. The result also clearly exhibits an asymmetry in the output power. This phenomenon results from a phase shift that the reflected field experiences as it is coupled into the laser cavity. The phase shift is dependent on the optical path difference as a result of change in the gap width. Therefore, the coupling coefficient is a complex function of the gap width consisting of an amplitude reduction term and a phase shift term. The degree of asymmetry rises with an increase of the reflectivity of the target surface. In contrast, in the absence of the phase shift, the peak of the signal will locate at the relative position of 0.25λ, i.e. the output power is a symmetric curve. Consequently, the asymmetry in the signal also identifies the moving direction of the target surface. Moreover, the slope of the signal, the sensitivity of the signal to the position variation and also the minimum displacement resolution that the sensing probe can achieve, is obtained by finding the derivative of the signal function. This characteristic implies that the deeper the slope of the signal is, the finer the displacement resolution is. Calculated position accuracy can theoretically be as low as 2 nm, which is competitive with other control methods.

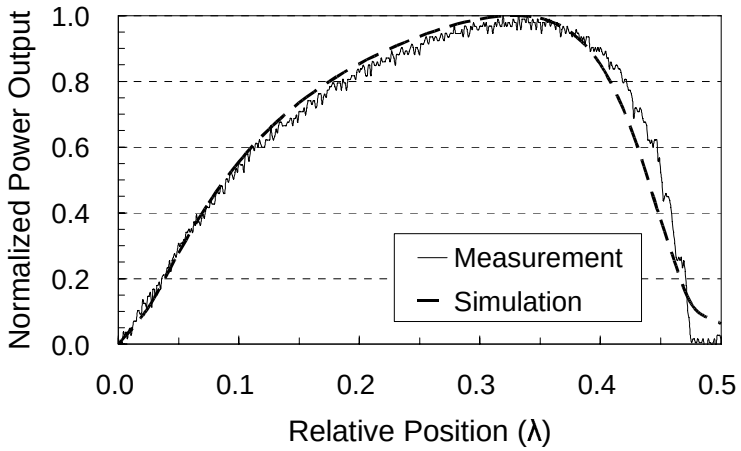

Fig. 5. Comparison of a measured feedback signal and a calculated self-mixing interferometric signal

The near-field gap control system consists of a laser diode, a fiber sensing probe, an actuator, drive circuits, and a controller. The emitted light from the laser diode is coupled into the fiber and delivered to the fiber end which functions as a position sensor. The variation in the gap width between the fiber end and the target surface alters the monitoring output power detected by the photodiode inside the laser diode. The modulation on output power is converted into a voltage signal and sent to the controller. A proportional integral (PI) controller is designed to actuate the real-time movement of the pickup and a lead compensator is integrated into the controller to improve phase and gain margins. A pickup driver and a signal amplifier are also designed accordingly to drive the actuator and suppress noise. The configuration of the system is shown in Fig. 6.

#84512 - $15.00 USD Received 25 Jun 2007; revised 31 Aug 2007; accepted 6 Sep 2007; published 22 Oct 2007

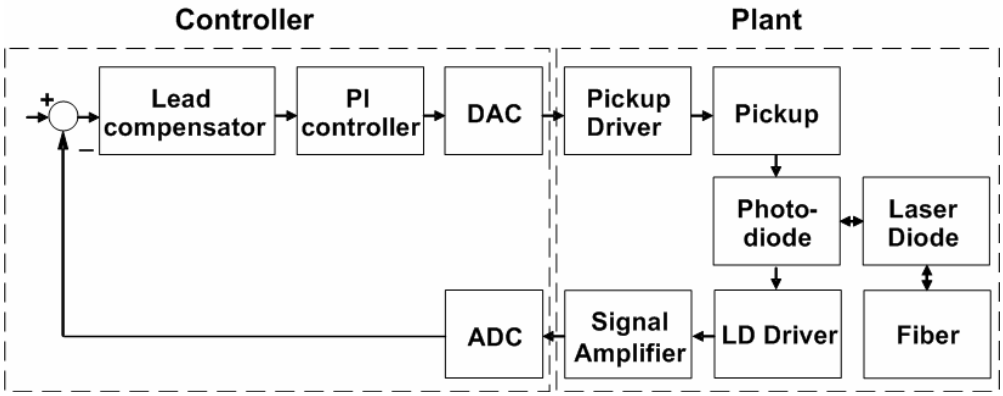

Fig. 6. Block diagram of the gap control system

3. Experiment and Results

3.1 Straw-shaped Writing Probe

According to the design, a 45-degree straw-shaped fiber probe was fabricated by a diamond sawing process, as shown in Fig. 7(a). A 200-nm silver film was deposited on the end face of the fiber probe by using a sputtering process and perforated with a C-aperture, of which the dimensions are shown in Fig. 7(b), by focused ion beam milling (FIB). Limited by the resolution of FIB, the outer dimension of the fabricated C-aperture is 300 nm (H) × 200 nm (W) while the line width is 100 nm. A 633-nm laser beam was coupled into the fiber probe and then the near-field intensity distribution of the fiber probe in the plane parallel to the end face was measured by a near-field scanning optical microscope (NSOM). Because the spatial resolution is worse than 50 nm, the measured spot size at a distance of 50 nm from the aperture is over 400 nm, which is larger than the simulated one. Moreover, since the measurement was carried out under the same set-up, the relative optical intensity emitted from the waveguide was represented by the signal amplitude. Compared to the signal amplitude of 0.02 V in the case of a circular aperture with a diameter of 100 nm, the straw-shaped fiber probe with the amplitude of 2 V yields the peak intensity enhancement by a factor of 10^2 higher than conventional probes.

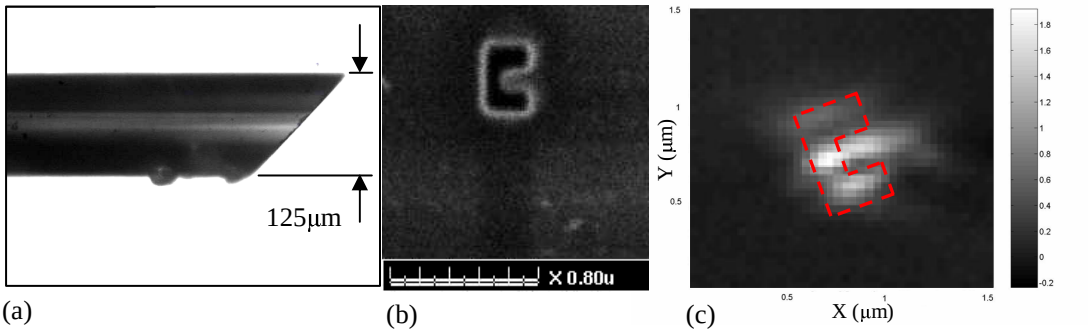

Fig. 7. (a). Optical microscopic photo of a 45-degree straw-shaped fiber probe, (b) SEM photo of the C-aperture on the end face of the fiber probe, and (c) near-field intensity distribution measured by NSOM

#84512 - $15.00 USD Received 25 Jun 2007; revised 31 Aug 2007; accepted 6 Sep 2007; published 22 Oct 2007

3.2 Gap Sensing Probe

To model the gap servo control system, the open-loop frequency response of components, including the biaxial actuator and the drive circuits, was measured and characterized by transfer functions. The controller was designed and fabricated consequently according to the system requirements. The open-loop frequency response of the entire system was then measured and compared with the design target which was numerically derived from control theory and the transfer functions. From the measurement results, we found that with the increase of frequency, the displacement of the actuator driven by the control system was attenuated. When the driving frequency was over 2×10^3Hz, the displacement became smaller than the resolution of the laser interferometer. Consequently, the measurement error increased and resulted in a black spot in the curve. Although the measurement precision degraded in high-frequency region, the results plotted in Fig. 8 still exhibit agreement between the measurement and simulation. Compactness of the fiber sensing probe made it possible to install the fiber probe on a conventional biaxial actuator without degrading the dynamic response. The phase and gain margin of this system was as high as 52° and -24 dB, respectively. The system was tested by moving the gap sensing probe toward the target surface within a distance of couples of wavelength under an actuated surface with displacement of 5 μm. If the amplitude gain from the photo-diode to the signal amplifier is G V/V, the sensitivity of the laser sensor is S V/nm, and the amplitude of the error signal is A V, the residual position error can be obtained by $A/(S\times G)$. According to this simply calculation, the experimental result shown in Fig. 9 clearly exhibits that the residual position error is maintained within ±1.5 nm in the case of A=6 mV/nm and S=32 V/V, which is close to the designed target of ±1 nm.

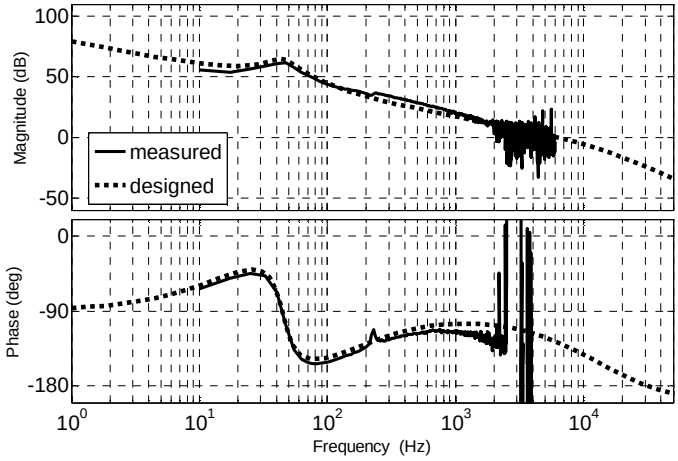

Fig. 8. Frequency response of the control system

#84512 - $15.00 USD Received 25 Jun 2007; revised 31 Aug 2007; accepted 6 Sep 2007; published 22 Oct 2007

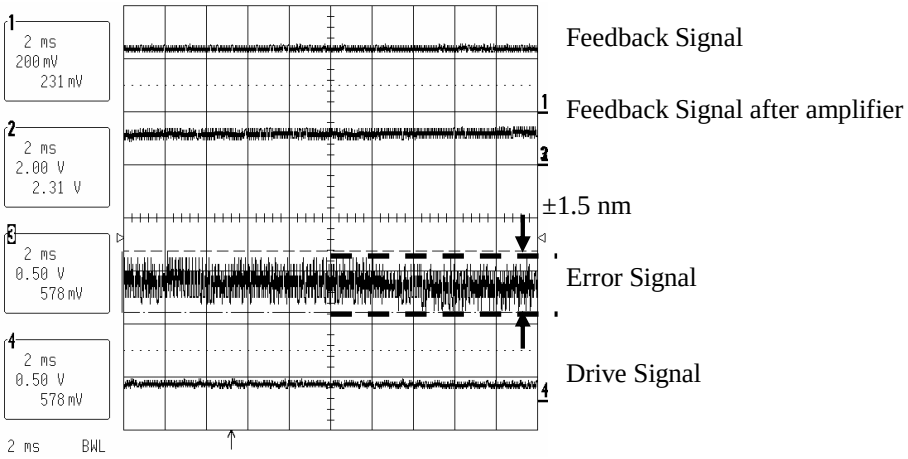

Fig. 9. Experimental result when the axial runout was 5 μm

4. Conclusions

We demonstrated a near-field fiber head system comprised of a straw-shaped writing probe which provided high power throughput employing the hybrid effect and a gap sensing probe which functioned as a position sensor and modulated the output power of the laser diode using self-mixing interferometric effect. We designed and demonstrated the straw-shaped writing probe and the gap sensing probe on a conventional biaxial actuator. The advantages of high transmission, compactness, achievability, and integration make this system competitive and provide a novel approach to near-field applications, including data storage, optical measurement, and lithography.

Acknowledgments

This research is partially supported by the National Science Council, Taiwan, for Promoting Academic Excellence of the University in "Photonics Science and Technology for Tera Era," under grant NSC 96-2752-E-009-009-PAE.

#84512 - $15.00 USD Received 25 Jun 2007; revised 31 Aug 2007; accepted 6 Sep 2007; published 22 Oct 2007